

Fractography Analysis with Topographical Features of Multi-Layer Graphene Reinforced Epoxy Nanocomposites

Rasheed Atif, Fawad Inam*

Department of Mechanical and Construction Engineering, Faculty of Engineering and Environment, Northumbria University, Newcastle, UK

Email: *fawad.inam@northumbria.ac.uk

How to cite this paper: Atif, R. and Inam, F. (2016) Fractography Analysis with Topographical Features of Multi-Layer Graphene Reinforced Epoxy Nanocomposites. *Graphene*, 5, 166-177.
<http://dx.doi.org/10.4236/graphene.2016.54014>

Received: August 30, 2016

Accepted: September 27, 2016

Published: September 30, 2016

Copyright © 2016 by authors and Scientific Research Publishing Inc. This work is licensed under the Creative Commons Attribution International License (CC BY 4.0).

<http://creativecommons.org/licenses/by/4.0/>



Open Access

Abstract

The stiff and fragile structure of thermosetting polymers, such as epoxy, accomplishes the innate cracks to cause fracture and therefore the applications of monolithic epoxy are not ubiquitous. However, it is well established that when reinforced especially by nano-fillers, its ability to withstand crack propagation is propitiously improved. The crack is either deflected or bifurcated when interacting with strong nano-filler such as Multi-Layer Graphene (MLG). Due to the deflection and bifurcation of cracks, specific fracture patterns are observed. Although these fracture patterns seem aesthetically appealing, however, if delved deeper, they can further be used to estimate the influence of nano-filler on the mechanical properties. Here we show that, by a meticulous examination of topographical features of fractured patterns, various important aspects related to fillers can be approximated such as dispersion state, interfacial interactions, presence of agglomerates, and overall influence of the incorporation of filler on the mechanical properties of nanocomposites.

Keywords

Fractography, Multi-Layer Graphene (MLG), Epoxy, Nanocomposites, Mechanical Properties

1. Introduction

The polymer matrix composites (PMCs) have found extensive applications in aerospace, automobile, and construction owing to ease of processing and high strength to weight ratio which is an important property required for aerospace applications [1]. Among different polymers, epoxy is the most commonly used thermosetting polymer

matrix in PMCs [2]. The damage tolerance and fracture toughness of epoxy can be enhanced with the incorporation of (nano-) fillers such as metallic oxides [3]-[5], clays [6]-[8], carbon nanotubes (CNTs) [9]-[11], and other carbonaceous materials [12]-[16]. After the groundbreaking experiments on the two-dimensional material graphene by Nobel Laureates, Sir Andre Geim and Konstantin Novoselov from the University of Manchester, graphene came into limelight in research field mainly because of its excellent electrical [17], thermal [18], and mechanical properties [19]. Graphene found widespread applications in electronics [20], bio-electric sensors [21], energy technology [22], lithium batteries [23], aerospace [24], bio-engineering [25], and various other fields of nanotechnology [26].

Non-contact techniques are getting increasingly popular to measure topographical features, especially for surfaces that may be subject to damage using contact techniques. The results obtained are very similar to those of stylus techniques and can use the same parameter definitions. Some non-contact techniques, such as diffraction measurements, can measure topographical features easily and quickly and can potentially be used on the machining tool. The non-contact methods have certain limitations. For example, in high slope surfaces, an insufficient intensity of light reaches the detector and the focus lens begins to follow inaccurately. In addition, when the contaminated surfaces are studied, the contamination is measured as part of topographical features as there is no external agency to remove the contaminations from the surface [27]. Considering these limitations, it was ensured that samples are placed flat and surface is clean to obviate any artefacts in topography profiles. In this work, an Alicona Infinite Focus optical microscope (G4) was used to measure topographical features. The Alicona optical microscope is a non-contact method (focus-follow method) for topography measurement. The focus-follow method involves the use of a moving lens which keeps a spot of light focused on the surface. The vertical movement of the lens is controlled by an electric motor and correlates to the surface profile [27]. The analog electrical signal is generated to drive the motor which is then digitized and processed in the same manner as a contact stylus. A separate transducer may also be used to monitor the position of the lens.

In current work, Multi-Layered Graphene (MLG)-epoxy nanocomposites of three different types were produced using solution casting technique with MLG dispersed in three different mediums: epoxy (ME), hardener (MH), and acetone (MA). The maximum improvement in mechanical properties was observed in case of MLG dispersed in hardener (MH) at 0.3 wt% MLG. The second highest improvement in mechanical properties was observed in case of MLG dispersed in epoxy (ME). However, in case of MLG dispersed in acetone (MA), least improvement in mechanical properties was observed. It can be attributed to the presence of retained acetone that causes stress concentration and concomitant degradation of mechanical properties [28]. The fractography analysis of the samples revealed that MLG significantly influences the fracture patterns. In addition, a careful examination of the topographical features of the fractured surfaces suggests that the dispersion state of the fillers, interfacial interactions, and presence of any agglomerates of filler can be estimated based on the surface parameters such as maxi-

mum surface roughness (R_z or R_{max}), surface roughness average (R_a), and root mean square parameter of roughness (R_q). For example, a high value of R_z with deep crater and/or trenches indicates the presence of filler agglomerates and concomitant poor mechanical properties of polymer nanocomposites. Similarly, a relatively high surface roughness average with low R_z value indicates the uniform dispersion of the filler and simultaneously improved mechanical properties. However, it was observed that waviness average parameter (W_a) does not have any relation with the weight fraction, dispersion state, or agglomeration of the filler.

2. Experimental Section

2.1. Materials

Multi-layered graphene (MLG) of 12 nm average thickness and 4.5 μm average lateral size with specific surface area of 80 m^2/g and purity 99.2% was purchased from Graphene Supermarket. MLG was washed extensively with acetone to remove any impurities and tip sonicated for 6 h to fragment any aggregates. Bisphenol A-epichlorohydrin based epoxy having density of $\sim 1.3 \text{ g/cm}^3$ and dimethylbenzylamine isophorone diamine based low viscosity fast curing hardener with $\sim 1.1 \text{ g/cm}^3$ density were used in current study. The epoxy matrix used consisted of EPOHENTM EL5 bisphenol A based liquid epoxy and EPOHENTM EHA57 diamine hardener, purchased from Polyfibre, UK. This epoxy system is a multi-purpose resin offering good all-round properties with the epoxy group content of 4.76 - 5.25 mol/kg. The viscosity of liquid epoxy and hardener are 12,000 - 15,000 cps and 45 cps at room temperature, respectively. To prepare monolithic epoxy samples, the mix proportions are 50 parts by weight of hardener to 100 parts by weight of liquid epoxy. The gelation time of the resin was 43 min at room temperature. Acetone of purity 99.8% was purchased from Sigma-Aldrich and was used as dispersion medium for MLG.

2.2. Samples Production

MLG of different weight fractions (0.1 wt%, 0.3 wt%, 0.5 wt% and 1.0 wt%) were taken and dispersed in three different mediums; (1) acetone (MA), (2) epoxy (ME), and (3) hardener (MH). The nano-filler was dispersed in the hardener using sonication that was carried out using tip sonicator of power 750 W and frequency 250 kHz (Vibra-cell model VC 750, USA). The operation mode was 70% power with 10 s vibration and 5 s break. Although the sonication was carried out at room temperature, however, temperature of the system rose due to high energy vibration produced by tip sonicator. The acetone was removed at 60°C for 2 h. The epoxy and hardener were vacuum degassed separately for 1 h. Then, the resins were mixed in epoxy: hardener ratio of 2:1. Following thorough hand mixing for 10 min, vacuum degassing was again carried out for 15 min. The resin was poured into silicone molds (without any release agent) and cured at room temperature for 6 h followed by post-curing at 150°C for overnight to ensure completion of the crosslinking.

2.3. Characterization

Tensile, three-point bending, and fracture toughness tests were conducted using Instron Universal Testing Machine (Model 3382). The displacement rate was kept 0.5 mm/min for tensile and fracture toughness tests and 1 mm/min for three-point bending test. Five specimens were tested for each composition. The schematics of the specimens are shown in **Figure 1**. Tensile properties were measured according to ASTM D638 Type-V geometry with specimen thickness 4 mm. Three-point bending test was conducted according to ASTM D790 with specimen dimensions $3 \times 12.7 \times 48$ mm. A single-edge-notch three-point bending (SEN-TPB) specimen was used to determine mode-I fracture toughness (K_{Ic}) according to ASTM D5045. The specimen dimensions were $3 \times 6 \times 36$ mm with a crack of length 3 mm. Charpy impact toughness test was carried out according to ASTM D6110 using notched specimen with dimensions $3.2 \times 12.7 \times 64$ mm. A V-notch (45°) was made in the middle of the specimen whose depth was 2.5 mm and tip of radius 0.25 mm. The specimen was placed as simply supported beam and hit by hammer from behind the notch.

3. Results and Discussion

The fractography specimens are shown in **Figure 2**. The monolithic epoxy showed straight bamboo-like fracture pattern indicating the occurrence of typical epoxy brittle fracture. It is because there are no crack bridging mechanisms available in monolithic epoxy. Therefore, once crack is initiated, it propagates without any diversions and results in straight fracture paths. However, with the incorporation of carbonaceous rein-

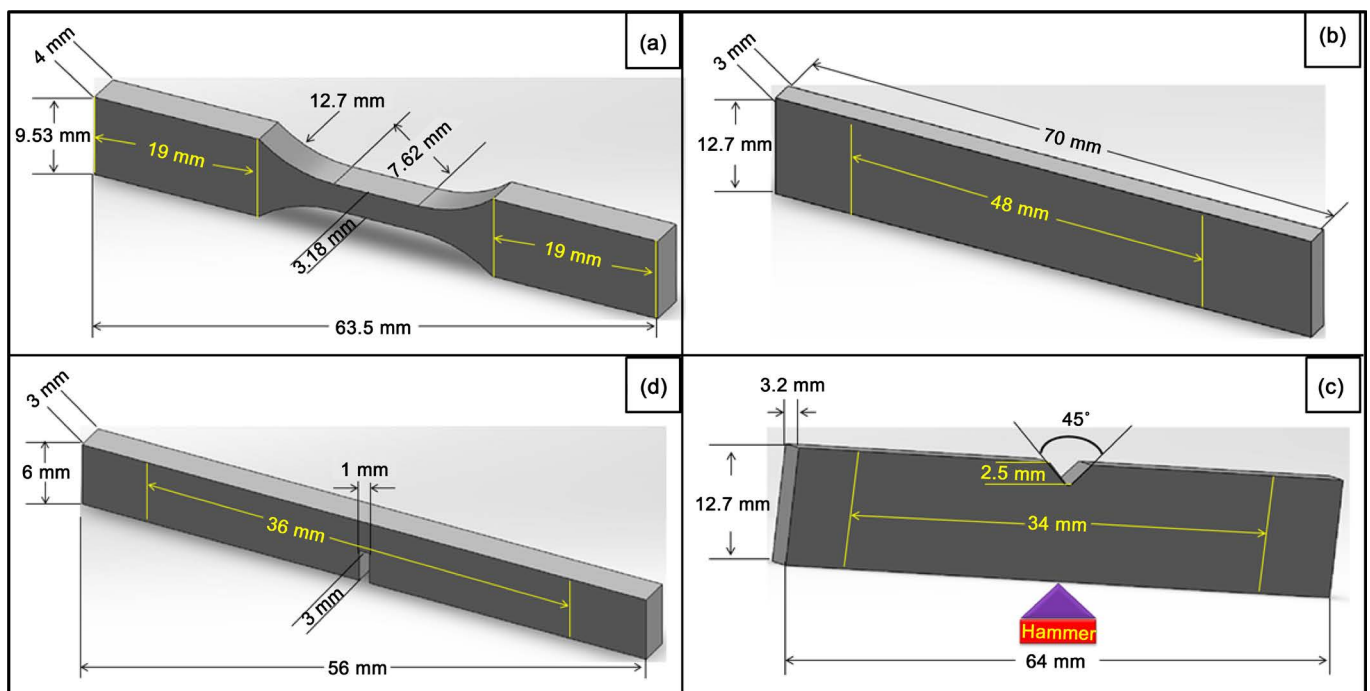


Figure 1. Schematics of mechanical test specimens: (a) tensile, (b) three-point bend, (c) Charpy impact toughness, and (d) fracture toughness (K_{Ic}).

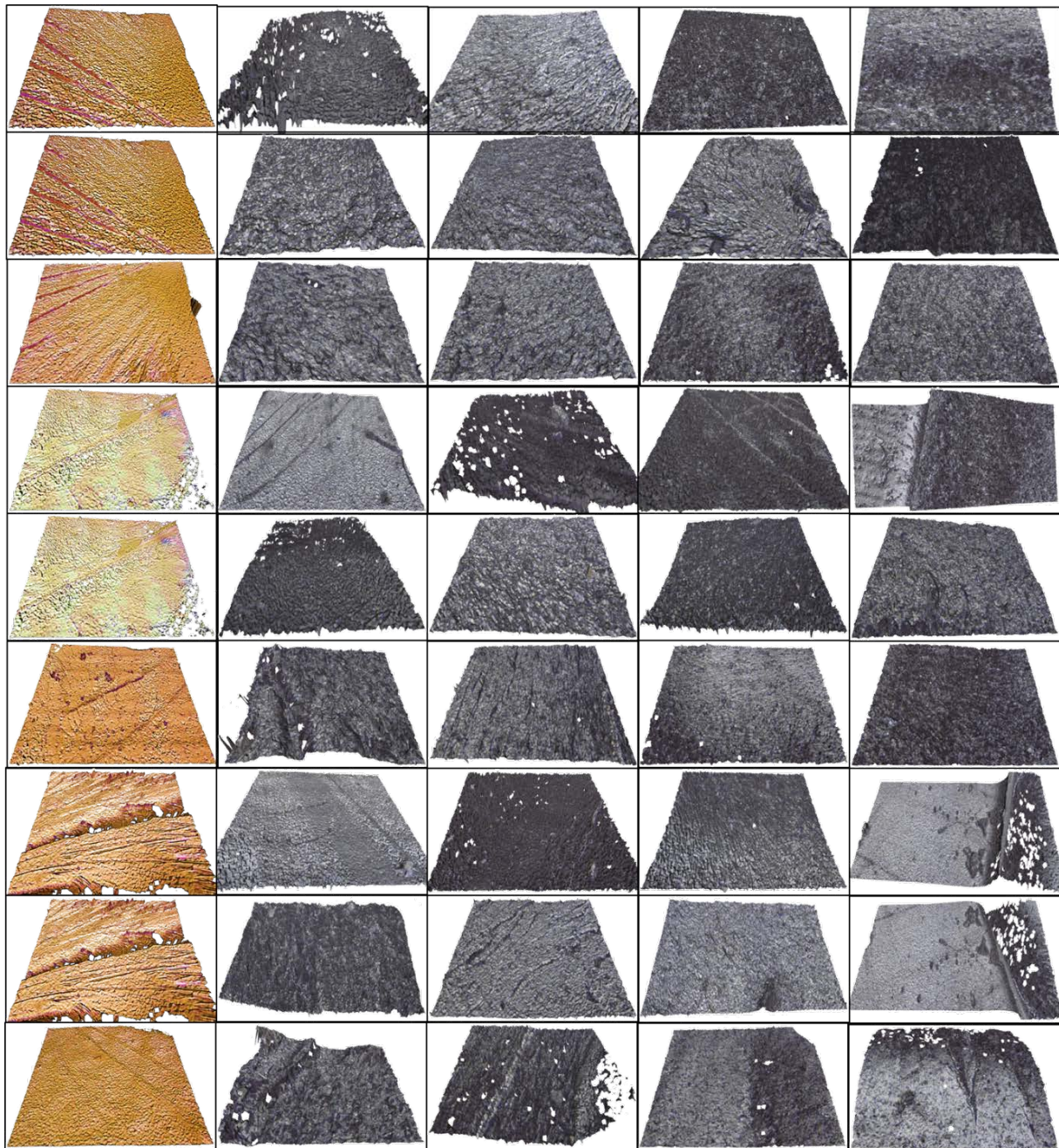


Figure 2. Fractured surfaces of 3PBT, K_{IC} , and Charpy impact test specimens. From left to right, the weight fraction of MLG varies as 0, 0.1, 0.3, 0.5, and 1.0 wt%, respectively. From top to bottom, the top three rows are 3PBT specimens, the middle three rows are K_{IC} specimens, and bottom three rows are Charpy impact toughness specimens (from top to bottom: ME, MH, and MA). The length of bottom edge of each image is 800 nm.

forcements, the cracks are deflected resulting in parabolic and non-linear fracture patterns [29]. This was the reason that no specific orientation of crack propagation was observed in 3PBT specimens reinforced with MLG. The fracture patterns of K_{IC} specimens differ from those of 3PBT specimens in a way that fracture was originated from the notch tip as the tip generated high levels of stress concentration. Although there

were no diversions in crack path in case of monolithic epoxy, however, a bit coarser topography was observed in case of MLG-EP samples. As the displacement rate is relatively low in K_{IC} testing, the MLG showed a significant impact on the topography of fracture surfaces. However, the influence of MLG on fracture patterns was marginalized in case of Charpy impact testing where the samples were suddenly impacted at the back of the notch by a heavy and pointed hammer. Sheer and straight fracture patterns were observed in Charpy impact specimens and fracture took place right from the notch tip in all cases. A slight increase in Charpy impact toughness with the incorporation of MLG indicates that MLG pull-out and fracture resulted in an increase in the force to cause fracture. The topographical features of fractured surfaces are further discussed below.

The topographical features of fracture surfaces of tensile specimen of ME are shown in **Figure 3**. Monolithic epoxy (**Figure 3(ai)**) showed typical straight fracture paths. On the other hand, no specific orientation of crack propagation was observed in 0.1 wt% ME (**Figure 3(bi)**). In addition, a coarse topography can be observed. A similar trend can be observed in 0.3 wt% ME (**Figure 3(ci)**). In case of 0.5 wt% ME (**Figure 3(di)**), craters and ravines can be observed that may arise from the agglomerates of MLG. It is interesting to note that tensile strength dropped at 0.5 wt% MLG and onwards compared to 0.1 wt% and 0.3 wt% ME samples. Therefore, it can be concluded that the dispersion state of MLG became inferior resulting in degradation in tensile strength due to stress concentration caused by agglomerates of MLG [30]. A relatively flat fracture pattern was observed in 1.0 wt% ME samples (**Figure 3(ei)**). A deep trench can be viewed

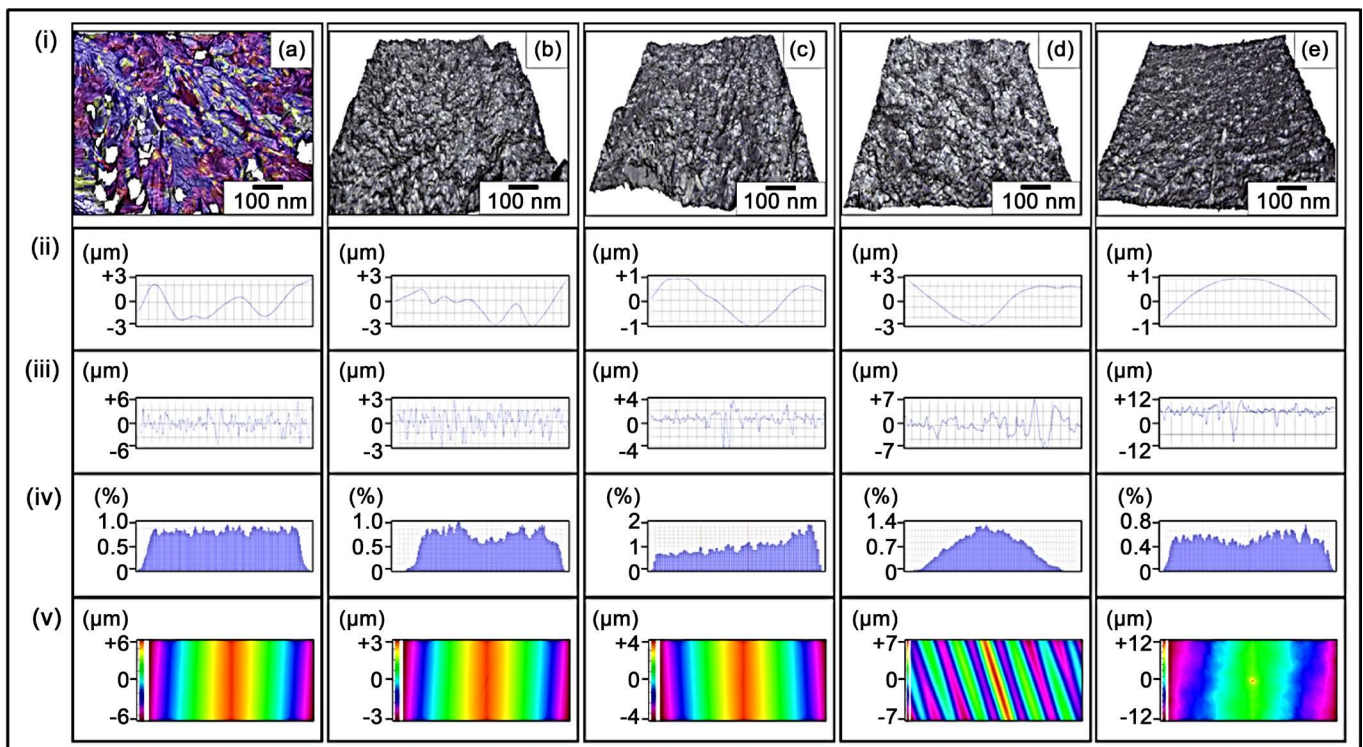


Figure 3. Topographical features of ME: (a) monolithic epoxy, (b) 0.1 wt% ME, (c) 0.3 wt% ME, (d) 0.5 wt% ME, and (e) 1.0 wt% ME. From top to bottom in all cases: (i) tensile images, (ii) waviness, (iii) roughness, (iv) Gaussian distribution, and (v) surface profile.

in **Figure 3(eiii)** that may arise from agglomerated MLG. This agglomerated MLG could possibly be the point of crack inception whose propagation could be precipitated by other agglomerated MLG regions resulting in rapid fracture and decreased tensile strength. The surface waviness (**Figure 3(ii)**) and Gaussian distribution (**Figure 3(iii)**) did not show a specific trend of change with MLG. It can be attributed to the multiple factors affecting the fracture pattern such as surface notches, MLG distribution, orientation, and interfacial interactions. Usually a specific pattern is observed in waviness due to wobbling of machining tool. On the contrary to W_a , a specific variation in surface roughness was observed. The surface roughness of monolithic epoxy varied between $\pm 6 \mu\text{m}$ with the presence of deep crests and troughs. With the incorporation of 0.1 wt% MLG, the surface roughness changed sharply indicating the crack being deflected by MLG at every step. A similar trend was observed in case of 0.3 wt% ME (**Figure 3(ciii)**). However, in case of 0.5 wt% and 1.0 wt% ME, deep trenches can be observed in roughness patterns (**Figure 3(diii)** and **Figure 3(eiii)**) that may be attributed to the presence of MLG agglomerates. The trenches can also be observed in the surface profiles (**Figure 3(dv)** and **Figure 3(ev)**). Similar trends were observed in cases of MH and MA as shown in **Figure 4** and **Figure 5**, respectively. However, a careful

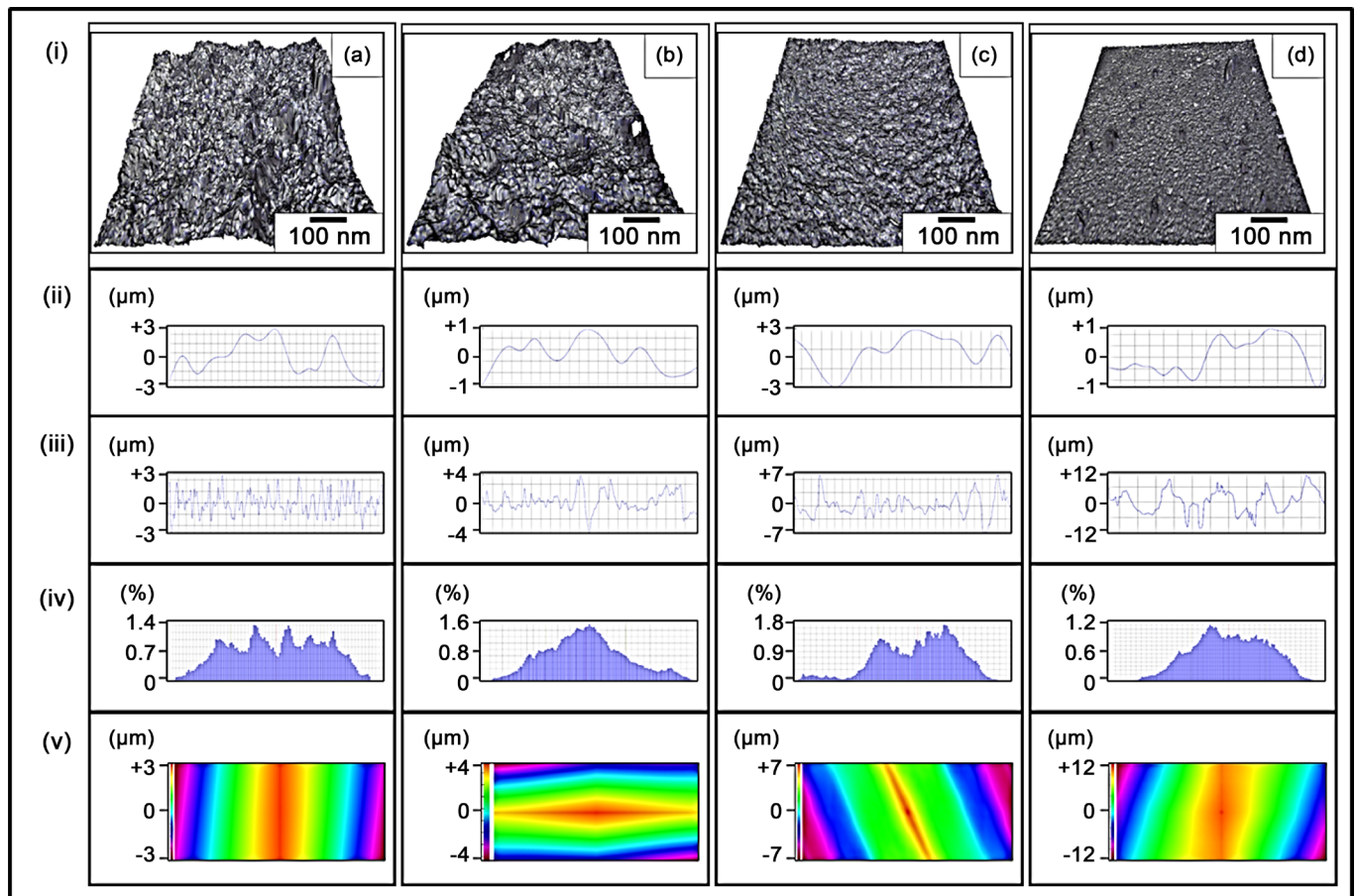


Figure 4. Topographical features of MH: (a) 0.1 wt% MH, (b) 0.3 wt% MH, (c) 0.5 wt% MH, and (d) 1.0 wt% MH. From top to bottom in all cases: (i) tensile images, (ii) waviness, (iii) roughness, (iv) Gaussian distribution, and (v) surface profile.

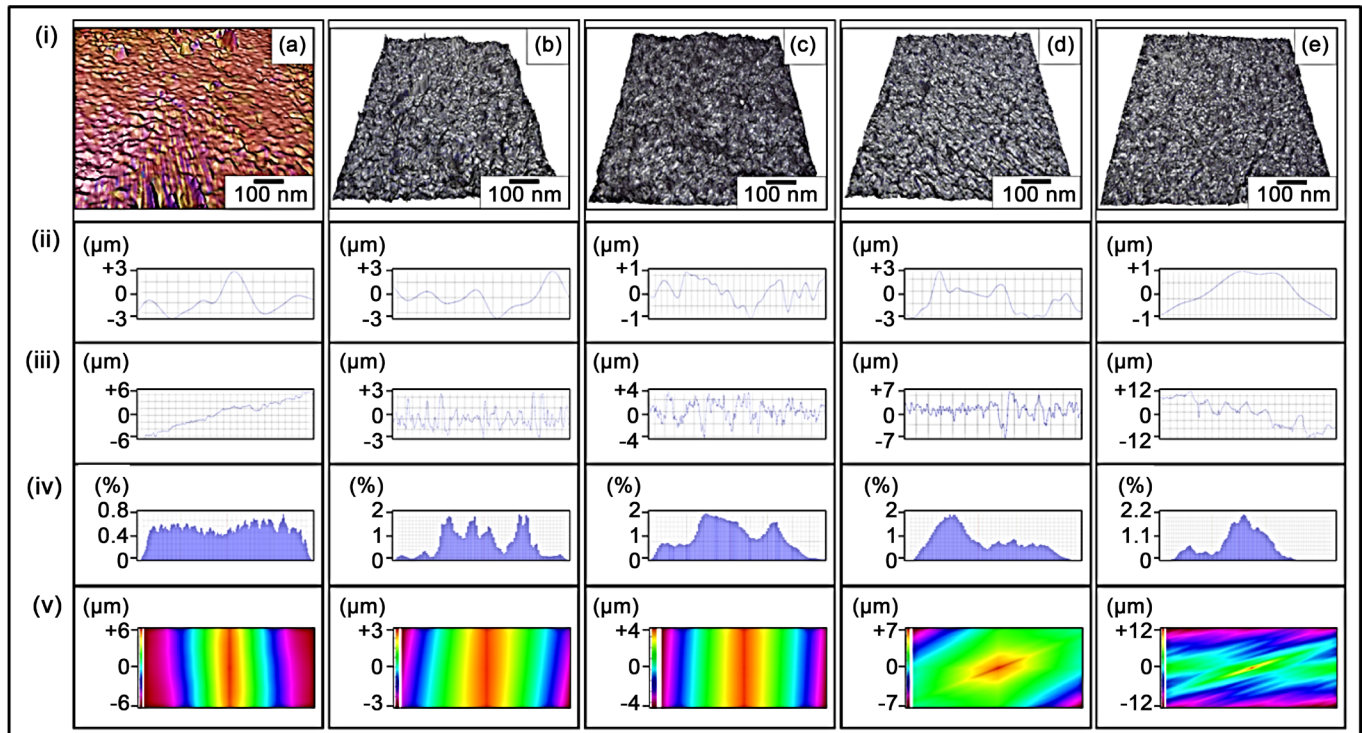


Figure 5. Topographical features of MA: (a) monolithic epoxy, (b) 0.1 wt% MA, (c) 0.3 wt% MA, (d) 0.5 wt% MA, and (e) 1.0 wt% MA. From top to bottom in all cases: (i) tensile images, (ii) waviness, (iii) roughness, (iv) Gaussian distribution, and (v) surface profile.

observation of topographical patterns can reveal some specific attributes of fracture patterns and distribution of MLG.

The topographical features are summarized in **Figure 6**. The R_z value of monolithic epoxy without acetone is $7.24 \mu\text{m}$ while with acetone is $6.47 \mu\text{m}$. This R_z comes from the ravines formed due to brittle fracture in the thermoset. The R_z values significantly decreased by the incorporation of MLG and became $4.44 \mu\text{m}$, $3.85 \mu\text{m}$, and $4.48 \mu\text{m}$ in 0.1 wt% ME, MH, and MA, respectively. The R_z values increased with increasing weight fraction of MLG. At 1.0 wt% MLG, the R_z values became $11.27 \mu\text{m}$, $9.68 \mu\text{m}$, and $10.31 \mu\text{m}$, respectively. As ravines were removed with the incorporation of 0.1 wt% MLG, and MLG divert the advancing cracks due to the reinforcing effect of MLG, therefore a decrease in R_z indicates a uniform dispersion of MLG and deflection of the cracks. In addition, an increase in mechanical properties at 0.1 wt% MLG in all cases further corroborates the uniform dispersion of MLG and energy dissipation at deflection of cracks. On the contrary, in 1.0 wt% MLG, the R_z values increased and were even higher than those in monolithic epoxy samples. No ravines were observed in 1.0 wt% MLG samples. Instead cracks and trenches were observed. Therefore, increase in R_z values and the presence of craters and trenches indicate that agglomerates of MLG were present that caused the fracture. A decrease in mechanical properties at 1.0 wt% MLG further corroborates the presence of agglomerates of MLG as agglomerated filler acts as stress concentration sites and causes fracture. Therefore, R_z can be an indicator of the dispersion state of filler.

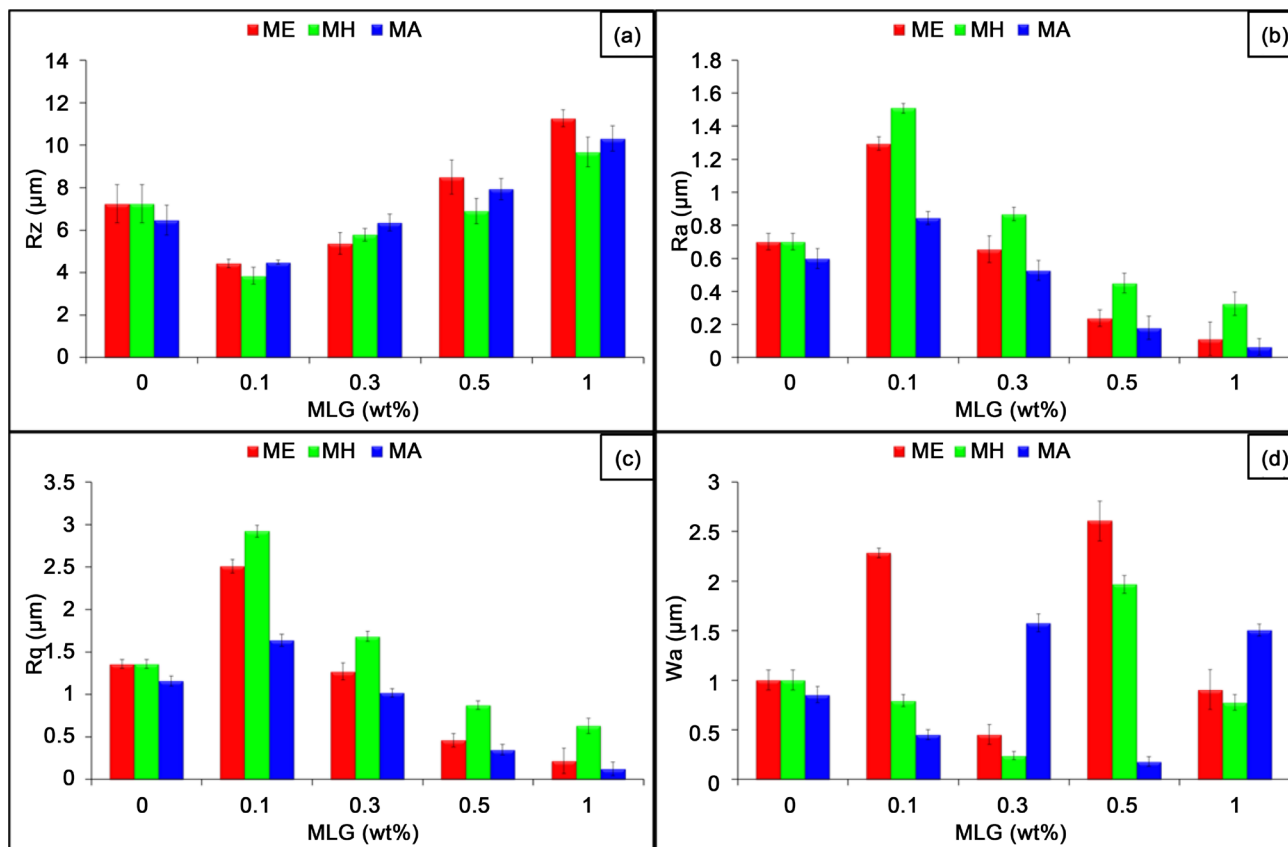


Figure 6. Topographical features of tensile specimens of ME, MH, and MA.

Apart from R_z , R_a is another important parameter to consider. The R_a values of monolithic epoxy without and with acetone are $0.7 \mu\text{m}$ and $0.61 \mu\text{m}$, respectively. With the addition of 0.1 wt\% MLG, the R_a values increased to $1.3 \mu\text{m}$, $1.51 \mu\text{m}$, and $0.85 \mu\text{m}$ in 0.1 wt\% ME, MH, and MA, respectively. However, on the contrary to R_z values, the R_a values decreased with the increasing weight fraction of MLG. At 1.0 wt\% MLG, the R_a values were $0.11 \mu\text{m}$, $0.33 \mu\text{m}$, and $0.06 \mu\text{m}$ in MA, MH, and MA, respectively. The decrease in R_a with increasing R_z may seem contradicting however can be explained on the basis of observed fractured patterns and surface roughness charts shown in **Figure 3** & **Figure 4**. At 0.1 wt\% MLG, due to uniform distribution of MLG, no crater was formed due to which lower R_z value was observed. In addition, cracks were deflected quite sharply resulting sudden variation in surface roughness thereby increasing the R_a value. On the contrary, at 1.0 wt\% MLG, agglomerates were present that caused fracture and increased R_z due to crater formation. However, once crack formed, it could not deflect much and rest of the fractured surface remained flat thereby decreasing the R_a value. Therefore, a high value of R_a (with low R_z value) can be an indicator of uniform dispersion of filler. On the other hand, a low value of R_a (with high R_z value) indicates the poor dispersion of filler and the presence of agglomerates. A similar trend was observed in R_q values as in R_a values. However, no specific trend was observed in surface waviness and may not be indicative of dispersion state.

4. Conclusion

The epoxy based nanocomposites were successfully produced with MLG as nano-filler. Three different systems were made with each system having five compositions. Fractography of samples from each composition was carried out and roughness parameters were analyzed. It was observed that the topographical features of fractured patterns of polymer nanocomposites can be used to approximate the dispersion state, interfacial interactions, and presence of agglomerates, and overall influence of the incorporation of fillers on the mechanical properties of produced nanocomposites. A high value of R_a (with low R_z value) can be an indicator of uniform dispersion of filler. On the other hand, a low value of R_a (with high R_z value) indicates the poor dispersion of filler and the presence of agglomerates. A similar trend was observed in R_q values as in R_a values. However, no specific trend was observed in surface waviness and may not be indicative of dispersion state.

Acknowledgements

The authors would like to thank the Department of Mechanical and Construction Engineering, Northumbria University, UK for the provision of research facilities, without which the analysis of relevant data was not possible.

References

- [1] Carlson, R.L., Kardomateas, G.A. and Craig, J.I. (2012) *Mechanics of Failure Mechanisms in Structures*. Springer, Berlin. <http://dx.doi.org/10.1007/978-94-007-4252-9>
- [2] Miracle, D.B. and Donaldson, S.L., Eds. (2001) *ASM Handbook, Vol. 21, Composites*. ASM International, Material Park, OH.
- [3] Yao, X.F., Zhou, D. and Yeh, H.Y. (2008) Macro/Microscopic Fracture Characterizations of SiO₂/Epoxy Nanocomposites. *Aerospace Science and Technology*, **12**, 223-230. <http://dx.doi.org/10.1016/j.ast.2007.03.005>
- [4] Wetzels, B., Rosso, P., Hauptert, F. and Friedrich, K. (2006) Epoxy Nanocomposites—Fracture and Toughening Mechanisms. *Engineering Fracture Mechanics*, **73**, 2375-2398. <http://dx.doi.org/10.1016/j.engfracmech.2006.05.018>
- [5] Naous, W., Yu, X.Y., Zhang, Q.X., Naito, K. and Kagawa, Y. (2006) Morphology, Tensile Properties, and Fracture Toughness of Epoxy/Al₂O₃ Nanocomposites. *Journal of Polymer Science Part B: Polymer Physics*, **44**, 1466-1473. <http://dx.doi.org/10.1002/polb.20800>
- [6] Kim, B.C., Park, S.W. and Lee, D.G. (2008) Fracture Toughness of the Nano-Particle Reinforced Epoxy Composite. *Composite Structures*, **86**, 69-77. <http://dx.doi.org/10.1016/j.compstruct.2008.03.005>
- [7] Wang, K., Chen, L., Wu, J., Toh, M.L., He, C. and Yee, A.F. (2005) Epoxy Nanocomposites with Highly Exfoliated Clay: Mechanical Properties and Fracture Mechanisms. *Macromolecules*, **38**, 788-800. <http://dx.doi.org/10.1021/ma048465n>
- [8] Liu, W., Hoa, S.V. and Pugh, M. (2005) Fracture Toughness and Water Uptake of High-Performance Epoxy/Nanoclay Nanocomposites. *Composites Science and Technology*, **65**, 2364-2373. <http://dx.doi.org/10.1016/j.compscitech.2005.06.007>
- [9] Gojny, F.H., Wichmann, M.H.G., Köpke, U., Fiedler, B. and Schulte, K. (2004) Carbon Nanotube-Reinforced Epoxy-Composites: Enhanced Stiffness and Fracture Toughness at

- Low Nanotube Content. *Composites Science and Technology*, **64**, 2363-2371.
<http://dx.doi.org/10.1016/j.compscitech.2004.04.002>
- [10] Yu, N., Zhang, Z.H. and He, S.Y. (2008) Fracture Toughness and Fatigue Life of MWCNT/Epoxy Composites. *Materials Science and Engineering: A*, **494**, 380-384.
<http://dx.doi.org/10.1016/j.msea.2008.04.051>
- [11] Srikanth, I., Kumar, S., Kumar, A., Ghosal, P. and Subrahmanyam, C. (2012) Effect of Amino Functionalized MWCNT on the Crosslink Density, Fracture Toughness of Epoxy and Mechanical Properties of carbon-Epoxy Composites. *Composites Part A: Applied Science and Manufacturing*, **43**, 2083-2086.
<http://dx.doi.org/10.1016/j.compositesa.2012.07.005>
- [12] Mathews, M.J. and Swanson, S.R. (2007) Characterization of the Interlaminar Fracture Toughness of a Laminated Carbon/Epoxy Composite. *Composites Science and Technology*, **67**, 1489-1498. <http://dx.doi.org/10.1016/j.compscitech.2006.07.035>
- [13] Arai, M., Noro, Y., Sugimoto, K. and Endo, M. (2008) Mode I and Mode II Interlaminar Fracture Toughness of CFRP Laminates Toughened by Carbon Nanofiber Interlayer. *Composites Science and Technology*, **68**, 516-525.
<http://dx.doi.org/10.1016/j.compscitech.2007.06.007>
- [14] Wong, D.W.Y., Lin, L., McGrail, P.T., Peijs, T. and Hogg, P.J. (2010) Improved Fracture Toughness of Carbon Fibre/Epoxy Composite Laminates Using Dissolvable Thermoplastic Fibres. *Composites Part A: Applied Science and Manufacturing*, **41**, 759-767.
<http://dx.doi.org/10.1016/j.compositesa.2010.02.008>
- [15] Atif, R., Shyha, I. and Inam, F. (2016) Modeling and Experimentation of Multi-Layered Nanostructured Graphene-Epoxy Nanocomposites for Enhanced Thermal and Mechanical Properties. *Journal of Composite Materials*, 1-12.
<http://dx.doi.org/10.1177/0021998316640060>
- [16] Atif, R. and Inam, F. (2016) Modeling and Simulation of Graphene Based Polymer Nanocomposites: Advances in the Last Decade. *Graphene*, **5**, 96-142.
<http://dx.doi.org/10.4236/graphene.2016.52011>
- [17] Pokharel, P., Truong, Q.-T. and Lee, D.S. (2014) Multi-Step Microwave Reduction of Graphite Oxide and Its Use in the Formation of Electrically Conductive Graphene/Epoxy Composites. *Composites Part B: Engineering*, **64**, 187-193.
<http://dx.doi.org/10.1016/j.compositesb.2014.04.013>
- [18] Tian, M., Qu, L., Zhang, X., Zhang, K., Zhu, S., Guo, X., *et al.* (2014) Enhanced Mechanical and Thermal Properties of Regenerated Cellulose/Graphene Composite Fibers. *Carbohydr Polym*, **111**, 456-462. <http://dx.doi.org/10.1016/j.carbpol.2014.05.016>
- [19] Xu, Z., Zhang, J., Shan, M., Li, Y., Li, B., Niu, J., *et al.* (2014) Organosilane-Functionalized Graphene Oxide for Enhanced Antifouling and Mechanical Properties of Polyvinylidene Fluoride Ultrafiltration Membranes. *Journal of Membrane Science*, **458**, 1-13.
<http://dx.doi.org/10.1016/j.memsci.2014.01.050>
- [20] Bkakri, R., Sayari, A., Shalaan, E., Wageh, S., Al-Ghamdi, A.A. and Bouazizi, A. (2014) Effects of the Graphene Doping Level on the Optical and Electrical Properties of ITO/P3HT, Graphene/Au Organic Solar Cells. *Superlattices and Microstructures*, **76**, 461-471.
<http://dx.doi.org/10.1016/j.spmi.2014.10.016>
- [21] Lian, Y., He, F., Wang, H. and Tong, F. (2014) A New Aptamer/Graphene Interdigitated Gold Electrode Piezoelectric Sensor for Rapid and Specific Detection of *Staphylococcus aureus*. *Biosensors & Bioelectronics*, **65**, 314-319. <http://dx.doi.org/10.1016/j.bios.2014.10.017>
- [22] Abdin, Z., Alim, M.A., Saidur, R., Islam, M.R., Rashmi, W., Mekhilef, S., *et al.* (2013) Solar

- Energy Harvesting with the Application of Nanotechnology. *Renewable & Sustainable Energy Reviews*, **26**, 837-852. <http://dx.doi.org/10.1016/j.rser.2013.06.023>
- [23] Sun, W., Hu, R., Liu, H., Zeng, M., Yang, L., Wang, H., *et al.* (2014) Embedding Nano-Silicon in Graphene Nanosheets by Plasma Assisted Milling for High Capacity Anode Materials in Lithium Ion Batteries. *Journal of Power Sources*, **268**, 610-618. <http://dx.doi.org/10.1016/j.jpowsour.2014.06.039>
- [24] Azeez, A.A., Rhee, K.Y., Park, S.J. and Hui, D. (2013) Epoxy Clay Nanocomposites—Processing, Properties and Applications: A Review. *Composites Part B: Engineering*, **45**, 308-320. <http://dx.doi.org/10.1016/j.compositesb.2012.04.012>
- [25] Aziz, A., Lim, H.N., Girei, S.H., Yaacob, M.H., Mahdi, M.A., Huang, N.M., *et al.* (2015) Silver/Graphene Nanocomposite-Modified Optical Fiber Sensor Platform for Ethanol Detection in Water Medium. *Sensors & Actuators B: Chemical*, **206**, 119-125. <http://dx.doi.org/10.1016/j.snb.2014.09.035>
- [26] Agnihotri, N., Chowdhury, A.D. and De, A. (2015) Non-Enzymatic Electrochemical Detection of Cholesterol Using β -Cyclodextrin Functionalized Graphene. *Biosensors & Bioelectronics*, **63**, 212-217. <http://dx.doi.org/10.1016/j.bios.2014.07.037>
- [27] Cotell, C.M., Sprague, J.A. and Smidth, F.A.J. (Eds.) (1994) ASM Handbook. Vol. 5, Surface Engineering. ASM International, Russell Township.
- [28] Atif, R., Shyha, I. and Inam, F. (2016) The Degradation of Mechanical Properties Due to Stress Concentration Caused by Retained Acetone in Epoxy Nanocomposites. *RSC Advances*, **6**, 34188-34197. <http://dx.doi.org/10.1039/C6RA00739B>
- [29] Kuo, W.-S., Tai, N.-H. and Chang, T.-W. (2013) Deformation and Fracture in Graphene Nanosheets. *Composites Part A: Applied Science and Manufacturing*, **51**, 56-61. <http://dx.doi.org/10.1016/j.compositesa.2013.03.020>
- [30] Atif, R., Wei, J., Shyha, I. and Inam, F. (2016) Use of Morphological Features of Carbonaceous Materials for Improved Mechanical Properties of Epoxy Nanocomposites. *RSC Advances*, **6**, 1351-1359. <http://dx.doi.org/10.1039/C5RA24039E>



Scientific Research Publishing

Submit or recommend next manuscript to SCIRP and we will provide best service for you:

Accepting pre-submission inquiries through Email, Facebook, LinkedIn, Twitter, etc.
 A wide selection of journals (inclusive of 9 subjects, more than 200 journals)
 Providing 24-hour high-quality service
 User-friendly online submission system
 Fair and swift peer-review system
 Efficient typesetting and proofreading procedure
 Display of the result of downloads and visits, as well as the number of cited articles
 Maximum dissemination of your research work

Submit your manuscript at: <http://papersubmission.scirp.org/>

Or contact graphene@scirp.org